Molecular Dipole-Induced Photoredox Catalysis for Hydrogen Evolution over Self-assembled Naphthalimide Nanoribbons

Huan Lin[1, 2, 3†], Junhui Wang[4†], Jiwu Zhao[1], Yan Zhuang[1], Bingqian Liu[1], Yujiao Zhu[2], Huaping Jia[2], Kaifeng Wu[4], Jinni Shen[1], Xianzhi Fu[1], Xuming Zhang[2*], Jinlin Long[1*]

[†]These authors contributed equally to this work.

[a] Dr. H. Lin, Dr. J. Zhao, Dr Y Zhuang, B. Liu, Prof. J. Shen, Prof. X. Fu, Prof. J. Long
State Key Laboratory of Photocatalysis on Energy and Environment,
College of Chemistry, Fuzhou University
Fuzhou 350108 (P. R. China)
E-mail: jllong@fzu.edu.cn
[b] Dr. H. Lin, Dr. Y. Zhu, Dr. H. Jia, Prof. X. Zhang
Department of Applied Physics
The Hong Kong Polytechnic University
Hong Kong 999077 (P. R. China)
E-mail: apzhang@polyu.edu.hk
[c] Dr. H. Lin
Beijing Key Laboratory for Green Catalysis and Separation,
Department of Environmental Chemical Engineering, Beijing University of Technology
Beijing 100124 (P. R. China)
[d] Prof. J. Wang, Prof. K. Wu
State Key Laboratory of Molecular Reaction Dynamics and Dynamics Research Center for Energy and Environmental Materials
Dalian Institute of Chemical Physics, Chinese Academy of Science
Dalian 116023 (P. R. China)

Abstract: D-π-A type 4-((9-phenylcarbazol-3-yl)ethynyl)-N-dodecyl-1,8-naphthalimide (CZNI) with a large dipole moment of 8.49 D and A-π-A type bis[(4,4'-1,8-naphthalimide)-N-dodecyl]ethyne (NINI) with a negligible dipole moment of 0.28 D, were smartly designed and synthesized to demonstrate the evidence of molecular dipole as the dominant mechanism for controlling charge separation of organic semiconductors. In aqueous solution, these two novel naphthalimides can self-assemble to nanoribbons (NRs) that present significantly different traces of exciton dissociation dynamics. Upon photoexcitation of NINI-NRs, no charge-separated excitons (CSEs) can be formed due to the large exciton binding energy, accordingly no hydrogen evolution. On the contrary, in the photoexcited CZNI-NRs, the initial bound Frenkel excitons are dissociated to long-lived CSEs after undergoing ultrafast charge transfer within *ca.* 1.25 *ps* and charge separation within less than 5.0 *ps*. Finally, these free electrons were injected to Pt co-catalysts for reducing protons to H_2 at a rate of *ca.* 417 μmol $h^{-1}g^{-1}$, correspondingly an apparent quantum efficiency of *ca.* 1.3% can be achieved at 400 nm.

Introduction

Making solar fuels through artificial photosynthesis has been considered as an appealing and sustainable strategy to relieve global reliance on non-renewable fossil fuels and concerns over environmental contamination.[1] Natural photosystems in plants and bacteria, where the π-stacked assemblies of light-absorbing pigments arrange themselves in configurations optimizing the ability to convert solar energy to chemical energy,[2] offered a voluminous of sources of bio-inspiration for designing artificial photoactive materials. The large mutual electronic and excitonic interactions between chromophores in these photosystems are essential for the broad light-harvesting capability, energy conversion and biological functions.[3] Therefore, mimicking the high delocalization of natural chromophore assemblies by creating novel organic semiconductors or dyes to construct highly-ordered supramolecular nanoarchitectures has been an active and exciting field developed recently for solar-to-chemical fuel conversion.

Among artificial chromophores, a majority of molecular organic semiconductors and dyes have been reported to be photocatalytically inactive, except that several polymeric semiconductors, perylene imides and porphyrins have the special functions for various charge-driven photoredox reactions.[4] It was mainly ascribed to the large exciton binding energy (E_b) related to the Coulomb potential between electron and hole,[5] which impaired severely the mobility of photogenerated charges and diminished the material functionality. Reducing E_b was thus the essential consideration for designing organic chromophores to construct supramolecular nanoarchitectures. Constructing donor-acceptor (D-A) configuration or interface was an effective strategy to reduce the Coulomb interaction of charge carriers by the formed internal electric field.[6] The energetic offset in the frontier orbitals of donor and acceptor can drive intermolecular charge transfer (CT) to form CT excitons (CTEs).[5a], [7] It was the critical step to avoid generation of excimers that are the leading actor of fast charge recombination[8], [9] Incorporating a π-bridge into D-A configurations can not only increase the separation distance between electron and hole, but distinctly enhance the electron delocalization.[10] It would make the initial bound Frenkel excitons (FEs) more easily dissociated to free charges due to the less Coulomb interaction.[5a] A fundamental understanding of free charge generation mechanism in D-π-A organic semiconductors was of most importance to unlock the kinetic bottleneck of solar-to-chemical fuel conversion, and yet has been missing up to date.

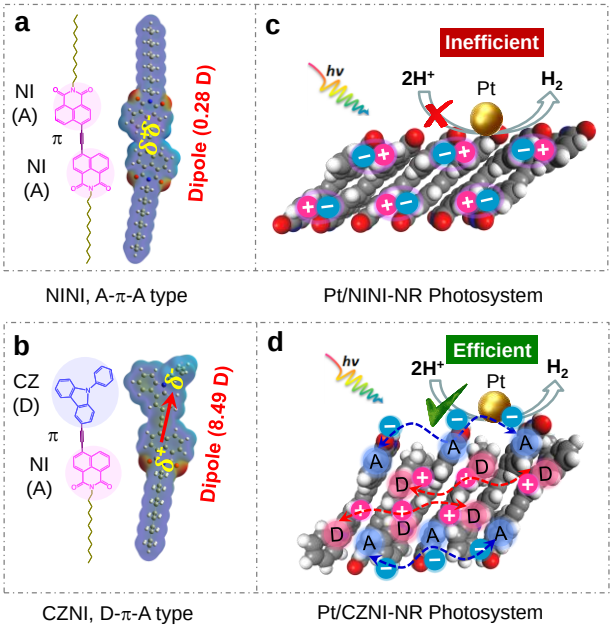

Figure 1. Molecular structures, dipoles and electron distribution of A-π-A type NINI (**a**) and D-π-A type CZNI (**b**). Schematic illustration of the self-assembled supramolecular NINI nanoribbon (NINI-NR) (**c**) and CZNI nanoribbon (CZNI-NR) (**d**) for photocatalytic hydrogen production with Pt nanoparticles as cocatalysts.

Herein, we designed two novel semiconducting naphthalimides to explore the keys to control the charge separation and transfer at a molecular level. One is bis[(4,4'-1,8-naphthalimide)-N-dodecyl]ethyne (denoted as NINI, Figure 1a) with the symmetrical A-π-A type configuration, which was synthesized by bridging of an ethynyl linker to two 1,8-naphthalimide (NI) units. Another is 4-((9-phenylcarbazol-3-yl)ethynyl)-N-dodecyl-1,8-napthalimide (denoted as CZNI, Figure 1b) with the asymmetrical D-π-A configuration, which was prepared by bridging of an ethynyl linker to the electron-deficient NI and electron-rich 9-phenylcarbazole (CZ) moieties.[11] The density functional theory (DFT) calculations showed that the former has a negligible dipole moment of *ca.* 0.28 D, while the energy offset of 1.86 eV between the LUMOs of CZ and NI units (Supporting Information, Figure S1) creates a large dipole moment of *ca.* 8.49 D to drive intramolecular charge transfer (CT) in the latter. The extended planar and rigid π-conjugated cores endowed them with a tendency to form self-assembled supramolecular nanoribbons. Especially, the alternating stacking of electron-rich moieties with electron-deficient units within self-assembled CZNI nanoribbons (CZNI-NR) can form a giant internal electric field to reduce the intermolecular charge-transfer energy.[12] Employing the femtosecond transient absorption spectroscopy (*fs*TA) and fluorescence spectroscopy, we succeeded in directly probing the key intermediates of intermolecular CT states in the photoexcited CZNI-NR. It was found that the bound FEs can be ultrafast dissociated to CTEs in lifetime of *ca.* 1.25 *ps*, and then converted to long-lived charge-separated excitons (CSEs) within *ca.* 4.86 *ps*. As expectedly, the photoexcited NINI-NRs did not demonstrate the same events because a majority (88%) of FEs radiatively decayed to the ground state and the remnants were converted to excimers that are the leading actor of fast charge recombination. No intermolecular CTEs formation made the Pt/NINI-NR photosystem inefficient for photocatalytic hydrogen evolution (Figure 1c). Amazingly, the bare CZNI-NRs did enable steady hydrogen production in the absence of any co-catalysts. The giant dipole field created two channels to conveniently transport free electrons and holes along the π-π stacking direction of CZNI-NRs (Figure 1d),[13] consequently protons were reduced by free electrons injected to the supported Pt nanoparticles (NPs) to H_2 at an average evolution rate of *ca.* 417 μmol $h^{-1}g^{-1}$. An impressive apparent quantum efficiency (AQE) of *ca.* 1.3% can be achieved with the Pt/CZNI-NR photosystem under 400 nm irradiation. This work offered the powerful evidence for the dipole-induced exciton dissociation for photoredox catalysis.

Results and Discussion

The synthesis of NINI and CZNI chromophores were described in detail in the Experimental Section in the Supporting Information. Owing to the π-π interaction, the NINI and CZNI monomers (denoted as NINI-M and CZNI-M, respectively) were orderly stacked and self-assembled to form supramolecular supramolecular nanoribbons. The atomic force microscopy (AFM) images (Figure 2a and 2b) displayed that both of them self-assembled into nanoribbons with have an ultrahigh aspect ratio of 100-300 nm width and dozens of microns length, further confirmed by the TEM and SEM results (Supporting Information, Figure S2). The height profile gave the average thickness of *ca.* 4.5 nm for NINI-NR, approximately equal to the molecular length of NINI (4.36 nm), implying that the π-π stacking of NINI aromatic cores is nearly perpendicular to the molecular plane, forming monolayer nanoribbons (Figure 2c and 2e). For CZNI-NR, the average thickness of *ca.* 13.0 nm is approximately equal to the thickness of 4-layer CZNI monomers (13.4 nm) (Figure 2d and 2e), suggesting the presence of the strong intermolecular interaction along all dimensions. The powder XRD and DFT simulation results (Supporting Information, Figure S3-S5) confirmed that the π-π stacking was slipped along the long dimension and arrayed side-by-side as a result of the weak intermolecular interaction between the crowded alkyl side chains of two NINI molecules (Figure 2c and Supporting Information,

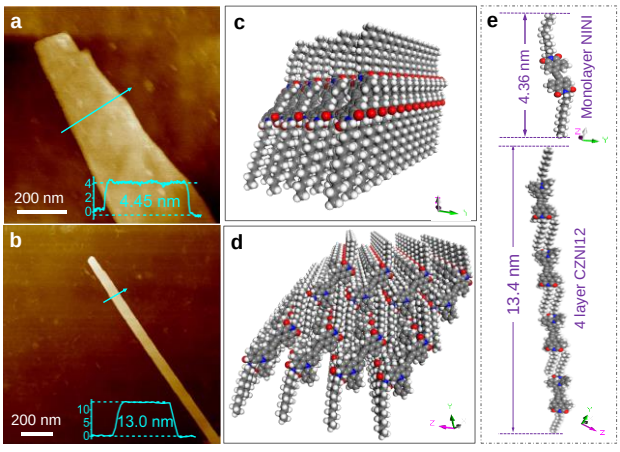

Figure 2. AFM images of the self-assembled NINI-NR (**a**) and CZNI-NR (**b**). Inset: Height profile along the cyan arrow in AFM image. The schematic representation of molecular packing within the NINI-NR (**c**) and CZNI-NR (**d**). (**e**) The height of monolayer NINI and four-layer CZNI with an orderly-packing model.

Figure S5 a-b). In contrast, the π-π stacking in CZNI-NR was interdigitated, as shown in Figure 2d and Supporting Information, Figure S5 c-d. The stronger intermolecular interaction between the CZ core and the NI ring facilitated the fast dissociation of excitons.

Next, we studied the giant difference in steady-state absorption and fluorescence spectra of the monomers and self-assembled nanoribbons, as showed in Figure 3. All the photophysical data were summarized in the Supporting Information, Table S1. It can appear from Figure 3a that owing to the strong vibrational interaction between the two closely-bound NI units, NINI-M displayed two vibronic bands centered at 421 and 397 nm, corresponding to the (0, 0) and (0, 1) π→π* electronic transitions, respectively.[14] Its emission bands were mirrored with the absorption features. It was ascribed to the formation of singlet excited state ^{1*}NINI.[14b, 15] CZNI-M gave an absorption band centered at 430 nm that was characterized by an emission band centered at 533 nm. The large photoluminescence (PL) Stokes shift of 103 nm (83 meV) suggested the occurrence of strong exciton-exchange interaction in CNZI-M.[16] Interestingly, the optical absorption of self-assembled nanoribbons was significantly broadened and red-shifted because of the inter-chromophore electronic coupling.[9] As shown in Figure 3b, an absorption edge occurred, respectively, at 490 and 537 nm for NINI-NR and CZNI-NR. A marked shoulder at 590 nm was observed for CZNI-NR, but its PL spectrum was highly consistent with the monomer. The different point is that the emission band at 533 nm was considerably quenched with a quantum yield (ϕ_F) of 28.3 %, greatly lower than its monomer (ϕ_F = 87 %) (Supporting Information, Table S1). Notably, except for the broad shoulder at *ca.* 700 nm, the NINI-NR retained the monomeric absorption features that were mirrored with the PL spectrum. It can appear that the emission bands were broaden and red-shifted into the region of 450-750 nm. The fluorescence quantum yield decreased to 19 %, relative to that of the monomer (ϕ_F = 84 %), attributed to the formation of excimer (Frenkel-CT exciton mixing).[17] No fluorescence emission bands belonging to the shoulder absorptions were discernible, indicating that the shoulder absorption bands were resulted from the extended charge transport and separation.[18]

The energy difference between the calculated transport gap energy ($E_g = |E_{HOMO}-E_{LUMO}|$) (Supporting Information, Figure S6) and the optical gap energy (E_{opt}) provides an approximation to the exciton binding energy ($E_b = E_g-E_{opt}$) (Figure 3c).[19] Thus, the E_b of CZNI-M was calculated to be 120 meV, which was much smaller than that (210 meV) of NINI-M. Furthermore, the E_b values of NINI-NR and CZNI-NR can be experimentally obtained by fitting the plot of the integrated PL intensity as a function of temperature (Figure 3d and Supporting Information, Figure S7) with the Arrhenius equation of $I(T) = I_0/(1+Ae^{(-E_b/k_BT)})$.[6b, 20] Accordingly, they were estimated to be 41 meV for CZNI-NR and 136 meV for NINI-NR, respectively. Compared to their monomers, the E_b was reduced significantly in the self-assembled nanoribbons due to the intermolecular exciton-exciton interaction. Especially, the E_b of 41 meV for CZNI-NR as low as some inorganic semiconductors enabled the fast dissociation of initial bound excitons into free charges,[21] which was further validated by the photoelectrochemical results shown in the Supporting Information, Figure S8. The much larger photocurrent response provided a powerful evidence for the efficient generation of free charges in the visible-light-excited CZNI-NR (λ ≥ 400 nm). These

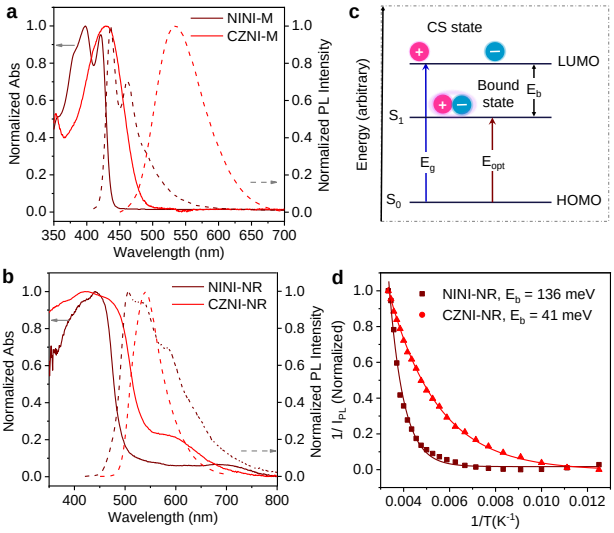

Figure 3. Normalized absorption (solid line) and PL (dashed line) spectra excited at 420 nm of NINI-M and CZNI-M in CH_2Cl_2 solution (20 μM) (**a**), as well as NINI-NR and CZNI-NR (**b**) in the solid state. (**c**) A free energy diagram showing the primary excitation species with different excitation energies. (**d**) The integrated PL intensity as a function of temperature to evaluate the exciton binding energy.

above-mentioned results confirmed clearly that the D-π-A configuration reduced drastically the exciton binding energy of naphthalimide-based semiconductors, thus maximizing the charge-separation efficiency.

To understand in-depth the generation mechanism of free charges within these self-assembled nanoribbons, femtosecond transient absorption (*fs*TA) spectroscopy was applied to study their initial photophysical events. As shown in the Supporting Information, Figure S9, photoexcitation of NINI-M mainly generated the singlet excited state ^{1*}NINI within 1.51 ± 0.32 *ps* due to the strong in-line excitonic coupling between two NI units (Supporting Information, Table S2).[22] The ^{1*}NINI species underwent the structural relaxation within τ_{rel} = 240 ± 39 *ps*, and then decayed to ground state in τ_F =1.86 ± 0.26 *ns*. Whereas, photoexcitation of CZNI-M (Supporting Information, Figure S10) led to the ultrafast intramolecular charge transfer (CT) within τ_{CT} =1.80 ± 0.13 *ps* to form the CT state ($CZ^{+\cdot}$-$NI^{-\cdot}$) owing to the intramolecular dipole field.[23] The CT state experienced the structural relaxation[24] within τ_{rel} = 180 ± 25 *ps* and decayed by charge recombination to ground state in τ_F = 4.02 ± 0.40 *ns* (Supporting Information, Table S2).

In the self-assembled nanoribbons, the interaction of an excited molecule with neighbors endowed reorganization of intermolecular distances and partial polarization of electronic configuration of the surrounding.[25] As shown in Figure 4a, the excited state absorption (ESA) spectra in early time window of NINI-NR were governed by the predominant bands at *ca.* 880 nm plus two weak absorptions centered at *ca.* 550 and 655 nm. These absorption bands were ascribed to the $S_n \leftarrow S_1$ transition of singlet Frenkel excitons (FEs). The decay of the ESA at 880 nm was accompanied by protruding of the weak absorption at 745 nm within 3.54 ± 0.21 *ps* (Supporting Information, Figure S11a, Table S2), which is an indicative of the formation of excimers in the closely-stacked NINI-NR.[26] Albeit, the absorption caused by the transition from lowest excimer state to a higher state with an ion-pair character in the NIR region of 1300-1600 nm[27] was indiscernible, suggesting that the formed excimers had a relatively low degree of charge-transfer character due to the large

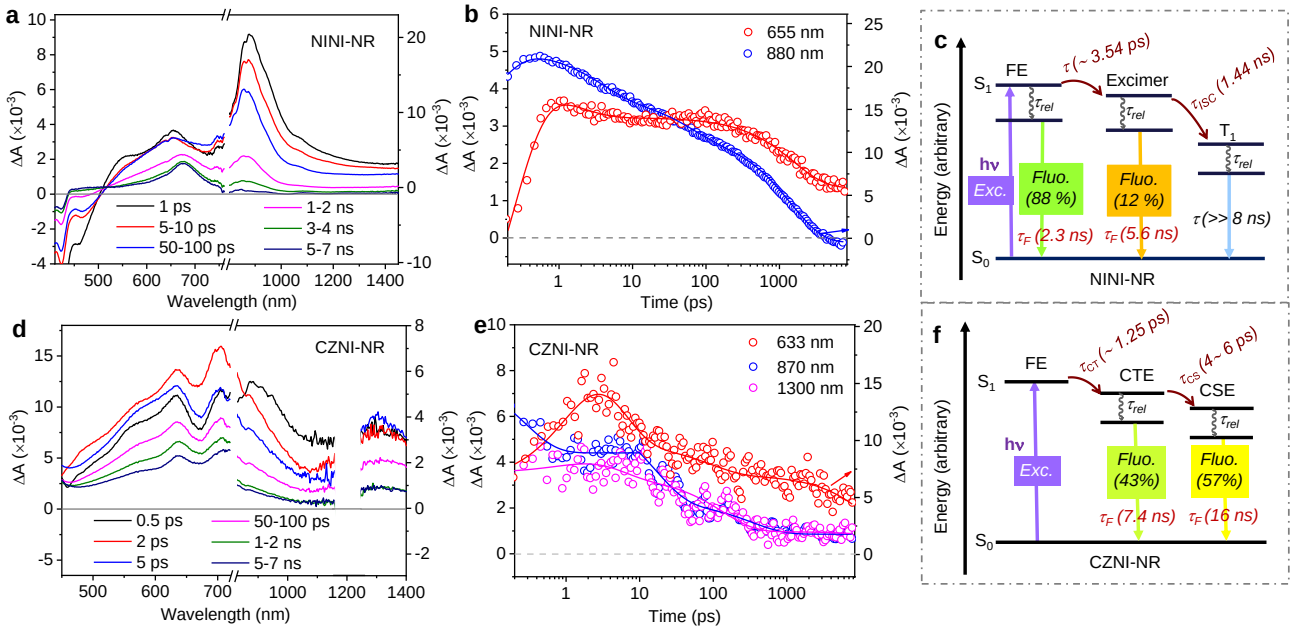

Figure 4. Femtosecond transient absorption (*fs*TA) spectra of NINI-NR in DMF/H_2O (9:1, v/v) (**a**) and CZNI-NR in CH_3OH/H_2O (1:9, v/v) (**d**). Kinetic trace plots of NINI-NR (**b**) and CZNI-NR (**e**) probed at selected wavelengths. The photophysical processes of photoexcited NINI-NR (**c**) and CZNI-NR (**f**).

exciton binding energy. The excimers subsequently decayed to yield triplet excitonic states with a long-lived (>> 8ns) board absorption at 675 nm by the intrinsic intersystem crossing (ISC) within 1.44 ± 0.28 *ns* (Figure 4b, and Supporting Information, Table S2).[28] The time-resolved fluorescence (TRF) spectrum of NINI-NR (Supporting Information, Figure S12) exhibited a bi-exponential decay with τ_{F1} = 2.26 *ns* (88%) and τ_{F2} = 5.55 *ns* (12%). The shorter lifetime corresponded to the decay of FEs to ground state, while the longer one was attributed to the excimer decay. The relevant photophysical processes of photoexcited NINI-NR was depicted clearly in Figure 4c.

Interestingly, the *fs*TA spectra of CZNI-NR were markedly different from those of NINI-NR, as shown in Figure 4d. The transient species at 870 nm attributed to singlet FEs suffered from a complete decay in 50-100 *ps*, while the excimer species at 633 and 705 nm were pronounced in 0.5-2.0 *ps*. Moreover, one absorption belonging to the intermolecular CTEs was clearly discerned at *ca.* 1300 nm.[14b, 27] Such results indicated the occurrence of intermolecular charge transfer and separation in the photoexcited CZNI-NR. The kinetic traces of these absorption bands were shown in Figure 4e and Supporting Information, Figure S11b. All the features exhibited a multi-exponential decay, and the fit results of the *fs*TA data were listed in the Supporting Information, Table S2. The three bands at 633, 705 and 1300 nm suffered from a similar triexponential decay dynamics. The lifetime of fast component (42-49%) was *ca.* 4.0-6.0 *ps*. It was resulted from fast charge separation to form CSEs that had a broad absorption band overlapped with that of CTEs at 1200-1400 nm.[29] The second one was attributed to the geometric rearrangement of CTEs in *ca.* 100 *ps*, followed by the dominant charge recombination in a long-lived lifetime of τ_3 > 8.0 *ns* without triplet excited state formation. After decay for 100 *ps*, the final structureless absorption spectra were represented in 450-1400 nm, suggesting that quantities of free or loosely-bound charge carriers were produced.[30] The PL results (Supporting Information, Figure S12) further confirmed the conclusions. The lifetime of two emission processes was τ_{F1} = 7.43 *ns* (43.0 %) and τ_{F2} = 16.0 *ns* (57.0 %), corresponding to CTEs and CSEs, respectively. The photogenerated charge dynamics of CZNI-NR was schematically depicted in Figure 4f. Expectedly, the formation of intermolecular CSEs will endow CZNI-NR unique photochemical functions for solar energy conversion.

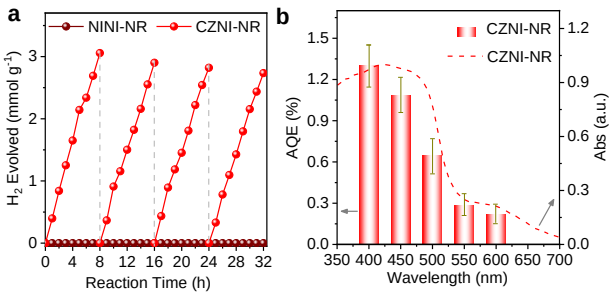

Figure 5. (**a**) Time course of H_2 evolutions on NINI-NR and CZNI-NR in water under visible light irradiation (λ ≥ 400 nm) for 32 h (four cycles), using in-situ photodeposited Pt (3.0 wt%) NPs as co-catalysts and TEOA (30% V/V) as sacrificial electron donor. (**b**) Wavelength-dependence AQE of photocatalytic H_2 evolution over CZNI-NR.

The positive slope of typical Mott-Schottky plots showed an n-type feature of NINI-NR and CZNI-NR (Supporting Information, Figure S13). The flat-band potentials of NINI-NR and CZNI-NR were determined to be -0.90 V and -1.40 V *vs* RHE, respectively. Thus, the valence band potentials were estimated to be +1.77 V *vs* RHE for NINI-NR and +0.95 V *vs* RHE for CZNI-NR. The results suggested that the photocatalytic reduction reaction of protons to H_2 was thermodynamically feasible under visible light irradiation (λ ≥ 400 nm), and the hole-driven oxidation reaction was able to take place over the two photocatalysts in the presence of triethanolamine (TEOA) as a sacrificial electron donor.[31] it can appear from Figure S14 (Supporting Information) that the bare CZNI-NR did enable steady hydrogen production at an average evolution rate of 21.8 μmol $h^{-1}g^{-1}$ in the absence of any co-catalysts, while the bare NINI-NR was photocatalytically inactive. After in-situ photodeposited Pt NPs over CZNI-NR, the H_2

evolution was significantly boosted, as shown in Figure 5a. Under the optimized reaction conditions (Supporting Information, Figure S15), the average rate of H_2 production was increased to *ca.* 417 μmol h^{-1} g^{-1}, while no hydrogen gas was detectable in the Pt/NINI-NR photosystem. The PXRD, SEM and TEM characterizations (Supporting Information, Figure S16 and 17) did not show any significant structural changes, except for the deposited Pt NPs, confirming the photochemical stability of NINI-NR and CZNI-NR. The H_2 evolution rate decreased slightly after 32 h, probably due to the consumption of the sacrificial electron donor (i.e., TEOA).[32] The apparent quantum efficiency (AQE) of CZNI-NR as a function of the incident light wavelength gave a well-matched action spectrum (Figure 5b), proving that the reaction was a light-driven redox catalytic process. The largest AQE of *ca.* 1.3 % for H_2 evolution was achieved at 400 nm. The time-resolved fluorescence kinetics (Supporting Information, Figure S18) further confirmed that the charge transfer occurred among TEOA, CZNI-NRs and Pt NPs, while the process did not proceed within the analogous NINI-NR photosystem. Such results indicated that the charge-driven photoredox catalysis for H_2 evolution was controlled essentially by the molecular dipole of organic semiconductors, which was responsible for the efficient and fast dissociation of FEs to free charges. From the viewpoint of catalysis, the H_2 evolution still was subjected to a slow mass transfer kinetics due to the high hydrophobicity (Supporting Information, Figure S19), a simple and effective strategy is to introduce some hydrophilic substituents such as -COOH and NH_4^+ to the alkyl chain end to improve the dispersity of CZNI-NR in aqueous solution.

Conclusion

In summary, two novel organic semiconductors, asymmetrical 4-((9-phenylcarbazol-3-yl)ethynyl)-1,8-naphthalimide with a large dipole moment of 8.49 D and symmetrical bis[(4,4'-1,8-naphthalimide)-N-dodecyl]ethyne with a negligible dipole moment of 0.28 D, were designed and synthesized to demonstrate the evidence and implication of molecular dipoles as the dominant mechanism for charge-driven photoredox catalysis. The exciton binding energy dominated by both of dipole moment and aggregate was one of the crucial parameters determining the dissociation of initially-bound Frenkel excitons into intermolecular charge-transferred excitons, finally to free charge carriers. The time-resolved transient absorption studies revealed that a large amount of long-lived charge-separated excitons (CSEs) with τ_F = 16.0 ns was generated upon photoexcitation of self-assembled CZNI-NRs, which was responsible for the stable photocatalytic H_2 evolution at an average rate of *ca.* 417 μmol h^{-1} g^{-1} under visible light irradiation. As a result, an impressive apparent quantum efficiency of *ca.* 1.3% at 400 nm was achieved with the Pt/CZNI-NR photosystem. In the analogous Pt/NINI-NR photosystem, no CSEs were formed, consequently no free charges drove the H_2 evolution. This work not only demonstrated one classical case of molecular dipole mediated redox photochemistry, but also offered a conceptual guidance for designing D-π-A type organic semiconductors with a large dipole to convert solar energy to hydrogen fuels or chemicals.

Acknowledgements

This work was financially supported from NSFC (Grants No. 22072022, 22011530144) and Research Grants Council of Hong Kong (Grants No. 15218415, 15212717, 15212618, 15221919E, 15215620E, N_PolyU511/20). J. Wang thanks the financial support from NSFC (21973091) and the Youth Innovation Promotion Association CAS (2021185).

Conflict of interest

The authors declare no conflict of interest.

Keywords: Photocatalysis • Molecular Dipole • Naphthalimide • Self-assembly • Hydrogen Evolution

[1] Z. Wang, C. Li, K. Domen, *Chem. Soc. Rev.* **2019**, *48*, 2109-2125.
[2] T. Pullerits, V. Sundström, *Acc. Chem. Res.* **1996**, *29*, 381-389.
[3] a) G. D. Scholes, G. R. Fleming, A. Olaya-Castro, R. Van Grondelle, *Nat. Chem.* **2011**, *3*, 763-774; b) O. Dumele, J. Chen, J. V. Passarelli, S. I. Stupp, *Adv. Mater.* **2020**, *32*, 1907247.
[4] a) J.-S. M. Lee, A. I. Cooper, *Chem. Rev.* **2020**, *120*, 2171-2214; b) S. Wu, Y. Pan, H. Lin, L. Li, X. Fu, J. Long, *ChemSusChem* **2021**, *14*, 4958-4972; c) A. S. Weingarten, R. V. Kazantsev, L. C. Palmer, M. McClendon, A. R. Koltonow, A. P. Samuel, D. J. Kiebala, M. R. Wasielewski, S. I. Stupp, *Nat. Chem.* **2014**, *6*, 964-970; d) R. V. Kazantsev, A. J. Dannenhoffer, T. Aytun, B. Harutyunyan, D. J. Fairfield, M. J. Bedzyk, S. I. Stupp, *Chem* **2018**, *4*, 1596-1608; e) Z. Zhang, Y. Zhu, X. Chen, H. Zhang, J. Wang, *Adv. Mater.* **2019**, *31*, 1806626; f) J. Ming, A. Liu, J. Zhao, P. Zhang, H. Huang, H. Lin, Z. Xu, X. Zhang, X. Wang, J. Hofkens, M. B. J. Roeffaers, J. Long, *Angew. Chem. Int. Ed.* **2019**, *58*, 18290-18294; *Angew. Chem.* **2019**, *131*, 18458-18462; g) D. Liu, J. Wang, X. Bai, R. Zong, Y. Zhu, *Adv. Mater.* **2016**, *28*, 7284-7290; h) Z. Zhang, X. Chen, H. Zhang, W. Liu, W. Zhu, Y. Zhu, *Adv. Mater.* **2020**, *32*, 1907746; h) J. Jing, J. Yang, W. Li, Z. Wu, Y. Zhu, *Adv. Mater.* **2021**, *33*, 210687; i) J. Yang, J. Jing, Y. Zhu, *Adv. Mater.* **2021**, *33*, 2101026; j) J. Wang, Y. Zhong, L. Wang, N. Zhang, R. Cao, K. Bian, L. Alarid, R. E. Haddad, F. Bai, H. Fan, *Nano Lett.* **2016**, *16*, 6523-6528.
[5] a) T. M. Clarke, J. R. Durrant, *Chem. Rev.* **2010**, *110*, 6736-6767; b) P. K. Nayak, *Synthetic Met.* **2013**, *174*, 42-45.
[6] a) K. Vandewal, S. Albrecht, E. T. Hoke, K. R. Graham, J. Widmer, J. D. Douglas, M. Schubert, W. R. Mateker, J. T. Bloking, G. F. Burkhard, *Nat. Mater.* **2014**, *13*, 63-68; b) Z. A. Lan, G. Zhang, X. Chen, Y. Zhang, K. A. Zhang, X. Wang, *Angew. Chem. Int. Ed.* **2019**, *58*, 10236-10240; *Angew. Chem.* **2019**, *131*, 10342-10346; c) G. B. Bodedla, G. Tang, J. Zhao, X. Zhu, *Sustainable Energy & Fuels* **2020**, *4*, 2675-2679; d) G. B. Bodedla, J. Huang, W.-Y. Wong, X. Zhu, *ACS Applied Nano Materials* **2020**, *3*, 7040-7046; e) G. B. Bodedla, W.-Y. Wong, X. Zhu, *J. Mater. Chem. A* **2021**, *9*, 20645-20652.
[7] M. Muntwiler, Q. Yang, W. A. Tisdale, X.-Y. Zhu, *Phys. Rew. Lett.* **2008**, *101*, 196403.
[8] C. Deibel, T. Strobel, V. Dyakonov, *Adv. Mater.* **2010**, *22*, 4097-4111.
[9] Y. L. Lin, M. A. Fusella, B. P. Rand, *Adv. Energy Mater.* **2018**, *8*, 1702816.
[10] M. Natali, S. Campagna, F. Scandola, *Chem. Soc. Rev.* **2014**, *43*, 4005-4018.
[11] D. Gudeika, J. V. Grazulevicius, D. Volyniuk, G. Juska, V. Jankauskas, G. Sini, *J. Phys. Chem. C* **2015**, *119*, 28335-28346.
[12] R. P. Fornari, A. Troisi, *Adv. Mater.* **2014**, *26*, 7627-7631.
[13] H. Geng, L. Zhu, Y. Yi, D. Zhu, Z. Shuai, *Chem. Mater.* **2019**, *31*, 6424-6434.
[14] a) Y. Liu, H.-Y. Wang, G. Chen, X.-P. Xu, S.-J. Ji, *Aust. J, Chem.* **2009**, *62*, 934-940; b) H. Lin, Z. Ma, J. Zhao, Y. Liu, J. Chen, J. Wang, K. Wu, H. Jia, X. Zhang, X. Cao, J. Long, *Angew. Chem. Int. Ed.* **2021**, *60*, 1235-1243; *Angew. Chem.* **2021**, *133*, 1255-1263.
[15] R. E. Cook, B. T. Phelan, R. J. Kamire, M. B. Majewski, R. M. Young, M. R. Wasielewski, *J. Phys. Chem. A* **2017**, *121*, 1607-1615.
[16] D. O. Demchenko, L.-W. Wang, *Phys. Rew. B* **2006**, *73*, 155326.

[17] R. J. Lindquist, K. M. Lefler, K. E. Brown, S. M. Dyar, E. A. Margulies, R. M. Young, M. R. Wasielewski, *J. Am. Chem. Soc.* **2014**, *136*, 14912-14923.

[18] E. H. Beckers, S. C. Meskers, A. P. Schenning, Z. Chen, F. Würthner, P. Marsal, D. Beljonne, J. Cornil, R. A. Janssen, *J. Am. Chem. Soc.* **2006**, *128*, 649-657.

[19] H. W. Li, Z. Guan, Y. Cheng, T. Lui, Q. Yang, C. S. Lee, S. Chen, S. W. Tsang, *Adv. Electron. Mater.* **2016**, *2*, 1600200.

[20] S. Sun, T. Salim, N. Mathews, M. Duchamp, C. Boothroyd, G. Xing, T. C. Sum, Y. M. Lam, *Energy Environ. Sci.* **2014**, *7*, 399-407.

[21] a) G. Karczewski, S. Maćkowski, M. Kutrowski, T. Wojtowicz, J. Kossut, *Appl. Phys. Lett.* **1999**, *74*, 3011-3013; b) P. Yu, X. Wen, Y.-R. Toh, J. Tang, *J. Phys. Chem. C* **2012**, *116*, 25552-25557.

[22] a) G. Duvanel, J. Grilj, A. Schuwey, A. Gossauer, E. Vauthey, *Photoch. Photobio, Sci.* **2007**, *6*, 956-963; b) M. I. Sluch, A. Godt, U. H. Bunz, M. A. Berg, *J. Am. Chem. Soc.* **2001**, *123*, 6447-6448.

[23] a) Y. Yang, S. R. Valandro, Z. Li, S. Kim, K. S. Schanze, *J. Phys. Chem. A* **2021**, *125*, 3863-3873; b) Y.-J. Cho, A.-R. Lee, S.-Y. Kim, M. Cho, W.-S. Han, H.-J. Son, D. W. Cho, S. O. Kang, *Phys. Chem. Chem. Phys.* **2016**, *18*, 22921-22928; c) R. Katoh, E. Katoh, N. Nakashima, M. Yuuki, M. Kotani, *J. Phys. Chem. A* **1997**, *101*, 7725-7728.

[24] J. M. Lim, P. Kim, M.-C. Yoon, J. Sung, V. Dehm, Z. Chen, F. Würthner, D. Kim, *Chem. Sci.* **2013**, *4*, 388-397.

[25] O. V. Mikhnenko, P. W. Blom, T.-Q. Nguyen, *Energy Environ. Sci.* **2015**, *8*, 1867-1888.

[26] M. Fujitsuka, S. S. Kim, C. Lu, S. Tojo, T. Majima, *J. Phys. Chem. B* **2015**, *119*, 7275-7282.

[27] E. A. Margulies, L. E. Shoer, S. W. Eaton, M. R. Wasielewski, *Phys. Chem. Chem. Phys.* **2014**, *16*, 23735-23742.

[28] K. M. Lefler, K. E. Brown, W. A. Salamant, S. M. Dyar, K. E. Knowles, M. R. Wasielewski, *J. Phys. Chem. A* **2013**, *117*, 10333-10345.

[29] T. Yoshihara, R. Katoh, A. Furube, Y. Tamaki, M. Murai, K. Hara, S. Murata, H. Arakawa, M. Tachiya, *J. Phys. Chem. B* **2004**, *108*, 3817-3823.

[30] K. Iwata, T. Takaya, H.-o. Hamaguchi, A. Yamakata, T.-a. Ishibashi, H. Onishi, H. Kuroda, *J. Phys. Chem. B* **2004**, *108*, 20233-20239.

[31] A. Celil Yüzer, E. Genc, E. Harputlu, G. Yanalak, E. Aslan, K. Ocakoglu, I. Hatay Patir, M. Ince, *Dalton Trans.* **2020**, *49*, 12550-12554.

[32] a) C. Yang, B. C. Ma, L. Zhang, S. Lin, S. Ghasimi, K. Landfester, K. A. I. Zhang, X. Wang, *Angew. Chem. Int. Ed.* **2016**, *55*, 9202-9206; *Angew. Chem.* **2016**, *128*, 9348-9352; b) W. Huang, Q. He, Y. Hu, Y. Li, *Angew. Chem. Int. Ed.* **2019**, *58*, 8676-8680; *Angew. Chem.* **2019**, *131*, 8768-8772.

Entry for the Table of Contents

The D-π-A type 4-((9-phenylcarbazol-3-yl)ethynyl)-N-dodecyl-1,8-naphthalimide (CZNI) with large dipole moment of 8.49 D was smartly designed and synthesized to fabricate self-assembled CZNI nanoribbons for efficiently photocatalytic hydrogen production. It was revealed that the molecular dipole field could significantly reduce the exciton binding energy of the organic semiconductor and drive exciton dissociation to free charges for reducing protons to H_2.